Mg^{2+}-dependent conformational rearrangements of CRISPR-Cas12a R-loop complex are mandatory for complete double-stranded DNA cleavage

Heyjin Son[a,1], Jaeil Park[a,1], Injoo Hwang[a], Youngri Jung[b], Sangsu Bae[b], and Sanghwa Lee[a,2]

[a]Advanced Photonics Research Institute, Gwangju Institute of Science and Technology, Gwangju 61005, Republic of Korea; and [b]Department of Chemistry, Hanyang University, Seoul 04763, Republic of Korea

Edited by Dana Carroll, The University of Utah, Salt Lake City, UT, and accepted October 29, 2021 (received for review July 26, 2021)

CRISPR-Cas12a, an RNA-guided DNA targeting endonuclease, has been widely used for genome editing and nucleic acid detection. As part of the essential processes for both of these applications, the two strands of double-stranded DNA are sequentially cleaved by a single catalytic site of Cas12a, but the mechanistic details that govern the generation of complete breaks in double-stranded DNA remain to be elucidated. Here, using single-molecule fluorescence resonance energy transfer assay, we identified two conformational intermediates that form consecutively following the initial cleavage of the nontarget strand. Specifically, these two intermediates are the result of further unwinding of the target DNA in the protospacer-adjacent motif (PAM)–distal region and the subsequent binding of the target strand to the catalytic site. Notably, the PAM-distal DNA unwound conformation was stabilized by Mg^{2+} ions, thereby significantly promoting the binding and cleavage of the target strand. These findings enabled us to propose a Mg^{2+}-dependent kinetic model for the mechanism whereby Cas12a achieves cleavage of the target DNA, highlighting the presence of conformational rearrangements for the complete cleavage of the double-stranded DNA target.

CRISPR-Cas12a | genome editing | single-molecule FRET | DNA cleavage | metal ion

CRISPR-Cas, a prokaryotic adaptive immune system, is a revolutionary tool for genome editing (1–6). Among the various types of the Cas systems, Cas12a (also known as Cpf1), class 2 type V-A CRISPR-Cas system, catalyzes double-stranded DNA (dsDNA) targets by utilizing single CRISPR RNA (crRNA) (7–10). The Cas12a-crRNA ribonucleoprotein (RNP) complex first identifies the dsDNA target via a T-rich protospacer-adjacent motif (PAM). Upon binding with cognate DNA, the Cas12a RNP unwinds the DNA via the formation of a crRNA-target strand (TS) heteroduplex and the simultaneous displacement of the nontarget strand (NTS) (a so-called R-loop structure) (11). Then, Cas12a generates double-strand DNA breaks with sticky ends by using a single RuvC nuclease domain in a sequential manner. Furthermore, in contrast to Cas9, Cas12a exhibits distinct features of pre-crRNA processing and indiscriminate single-stranded DNA cleavage activity (7, 12, 13). Owing to these unique features, CRISPR/Cas12a has been extensively utilized for the detection of nucleic acids as well as programmable genome editing (13–21).

Meanwhile, recently reported base and prime editors, which accomplish targeted edits in a highly efficient manner, utilized a nickase form of CRISPR/Cas9 to reduce the frequency of undesired insertions and deletions (22–24). However, the distinct feature by which both strands of target DNA are cleaved by a single catalytic site of Cas12a has hampered the development of engineered Cas12a RNPs including an efficient nickase, resulting in a limited range of Cas12a application (25–27). Given the advantages of Cas12a, including its multiplexing capability using the intrinsic crRNA processing activity and fewer off-target effects compared to Cas9 (14, 15, 17, 28), the development of various engineered Cas12a RNPs is necessary to improve genome editing techniques. Although recently several studies have suggested the nickase form of Cas12a RNPs using alterations of crRNA (29) or mutations of protein residues (30, 31), existing nickase variants still have much room for enhancement of the nicking activity. In this regard, thorough understanding of the mechanisms that regulate the sequential cleavage reaction of dsDNA, beginning with the NTS and proceeding to the TS, by a single catalytic site in the Cas12a RuvC domain, is required. However, despite many recent biochemical and structural studies (30–40), a detailed mechanistic understanding of the way in which Cas12a uses its single catalytic site to completely break the double strand of the target DNA is still lacking.

Here we perform single-molecule fluorescence assay to monitor conformational dynamics of the Cas12a ternary complex during TS cleavage following the initial cleavage of NTS of DNA. Recently, several groups have utilized similar methodological approaches to monitor the molecular interaction between Cas12a RNP and target DNA by using labeled target DNA and crRNA (35–37) and the interdomain dynamics of Cas12a protein by using labeled Cas12a (31, 41). Using this assay, here we identified the features of intermediates that form during conformational rearrangements in the TS cleavage reaction to complete dsDNA

Significance

CRISPR-Cas12a has emerged as attractive molecular scissors alternative to Cas9 owing to its unique features including fewer off-target effects, an alternative protospacer-adjacent motif sequence, pre-CRISPR RNA processing activity, and indiscriminate single-stranded DNase activity. However, despite these advantages, Cas12a has not been well utilized as recently reported base and prime editors because it does not have complete nickase variants, unlike Cas9. In this study, we provide a thorough understanding of the mechanisms that govern the generation of complete double-stranded DNA breaks by the single catalytic site of Cas12a using single-molecule fluorescence assays to improve our ability to develop a rational design for more potently engineered Cas12a including the nickase form. This would extend the range of genome editing applications of Cas12a.

Author contributions: H.S., J.P., and S.L. designed research; H.S., J.P., and I.H. performed research; Y.J. and S.B. contributed new reagents/analytic tools; H.S., J.P., and S.L. analyzed data; and H.S., J.P., and S.L. wrote the paper.

The authors declare no competing interest.

This article is a PNAS Direct Submission.

This open access article is distributed under Creative Commons Attribution-NonCommercial-NoDerivatives License 4.0 (CC BY-NC-ND).

[1]H.S. and J.P. contributed equally to this work.

[2]To whom correspondence may be addressed. Email: sanglee@gist.ac.kr.

This article contains supporting information online at http://www.pnas.org/lookup/suppl/doi:10.1073/pnas.2113747118/-/DCSupplemental.

Published December 1, 2021.

Downloaded by guest on December 5, 2021

cleavage and revealed its underlying mechanism based on a kinetic analysis of the conformational dynamics. The results of our study suggest that Mg^{2+}-mediated local DNA unwinding in the PAM-distal region is an essential prerequisite for the regulation of the sequential dsDNA cleavage reaction. This allosteric mechanism provides molecular insight into Cas12a engineering toward the development of Cas12a nickase.

Results

Independent Characterization of NTS and TS Cleavage Reactions by Cas12a RNPs. To investigate the differences between the NTS and TS DNA cleavage reactions by the same single catalytic site in the Cas12a RuvC domain, we observed the real-time conformational dynamics of the Cas12a–crRNA–DNA complex during the cleavage reactions for each strand using a single-molecule fluorescence resonance energy transfer (FRET) assay with prenicked DNA constructs (Fig. 1). As shown in Fig. 1*A*, we immobilized each DNA construct labeled with a FRET donor (Cy3) on a polymer-coated quartz surface using biotin–streptavidin interaction. Then, preassembled Cas12a–crRNA complexes labeled with a FRET acceptor (Cy5) were introduced while fluorescence signals from single Cas12a–crRNA–DNA complexes were monitored using a total internal reflection fluorescence microscope.

In the present study, for the independent detection of the NTS and TS cleavage reactions we used two types of DNA constructs: TS prenicked DNA (for NTS cleavage) and NTS prenicked DNA (for TS cleavage), which contain a nick in the scissile bonds of the TS and NTS, respectively (Fig. 1 *B* and *C*). Representative time traces showing the NTS and TS cleavage events in the prenicked DNA constructs are shown in Fig. 1 *D* and *E*. Upon addition of the Cas12a RNPs, the stable binding events of single Cas12a RNPs were detected by the appearance of the Cy5 signal in both DNA constructs. During the early stages of the binding events in both DNA constructs we obtained similar low FRET efficiencies, representing the R-loop complex (termed R-state hereafter) reported in our previous study (37). In the subsequent stage, however, the molecular behavior of the Cas12a RNP–DNA complex during the NTS and TS cleavage reactions differed significantly. In the NTS cleavage reaction, further FRET changes were not detected before the NTS strand was cleaved. However, in the TS cleavage reaction, the R-state (~0.21), which formed after the binding of Cas12a RNP, proceeded to subsequent steps through two distinct FRET states (~0.38 and ~0.59), after which the TS was eventually cleaved.

Previous structural studies have strongly suggested that the Cas12a complex may have to undergo large conformational changes to facilitate TS cleavage after first cleaving the NTS because Cas12a only has a single catalytic site for cleaving both of these strands (9, 31–33, 42). With this context in mind, the above observation regarding the two FRET changes observed only in the TS cleavage reaction is interpreted as reflecting the conformational rearrangements of the Cas12a RNP–DNA complex for the TS cleavage. On the basis of this result, we concluded

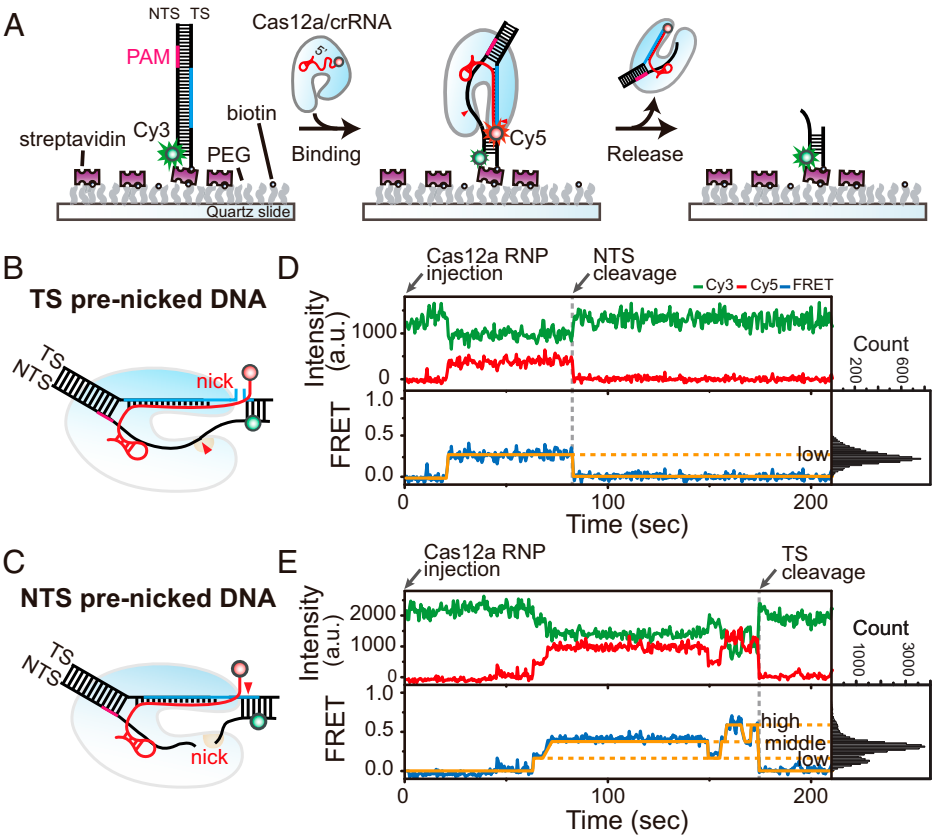


Fig. 1. Comparison of conformational dynamics between the NTS and TS cleavage reactions by Cas12a RNP. (*A*) Schematic diagram of single-molecule FRET experiment to monitor the cleavage reaction of nontarget and target DNA strands by Cas12a RNP. (*B* and *C*) Prenicked DNA constructs used for independent characterization of the cleavage reaction of the nontarget (*B*) TS prenicked DNA and target (*C*) NTS prenicked DNA) strands. (*D* and *E*) Representative time traces of Cy3 fluorescence (green, *Top*) and Cy5 fluorescence (red, *Top*), and corresponding FRET efficiency (blue, *Bottom*) in the presence of 20 nM Cas12a RNP for TS prenicked (*D*) and NTS prenicked (*E*) DNA constructs to show NTS and TS cleavage events, respectively. Corresponding FRET histograms are shown in the right panel of time traces. FRET histograms were obtained by collecting all data points from at least more than 60 time traces. Orange lines were added to guide the eye to allow clear visualization of the transitions. All FRET experiments in this figure were performed with Mg^{2+} concentration of 1 mM.

Downloaded by guest on December 5, 2021

that two consecutive conformational rearrangements of the Cas12a RNP–DNA complex are required for the TS cleavage reaction that follows the cleavage of NTS.

PAM-Distal DNA Unwinding and TS Binding to the Catalytic Site as Prerequisites for the TS Cleavage. Next, we aimed to assign the two subsequent FRET states observed in the TS cleavage reaction to structural and functional intermediates by using DNA constructs with various modifications. Recent crystal structures for the TS precleavage states of the Cas12a–crRNA–DNA complex indicate that the putative site of TS cleavage is located ~2.7 nm away from the catalytic site while maintaining base pairs with the complementary sequence of NTS (32). Thus, we infer that the unwinding of the double-stranded region containing the putative site of TS cleavage and the subsequent binding of the exposed TS cleavage site to the catalytic site of the RuvC domain are essential prerequisite steps for the TS cleavage. Consistent with this hypothesis, we observed two consecutive conformational rearrangements of the Cas12a ternary complex during the TS cleavage reaction. To test whether both of the observed conformational states correspond to the expected intermediates, we introduced various DNA modifications in the PAM-distal region of the target DNA and investigated the conformational dynamics compared with that of unmodified native DNA (Fig. 2 *A*–*C*). For the native NTS prenicked DNA at low Mg^{2+} concentration, we observed clear two-state dynamics between the low FRET (~0.21) and middle FRET (~0.38) states. The conformational equilibrium, however, was biased toward the middle FRET state when the PAM-distal region of the target DNA was preunwound (termed preunwound DNA) but was biased toward the low FRET state when oligonucleotides modified by locked nucleic acids were introduced to the PAM-distal region of the NTS to prevent the DNA unwinding (termed locked DNA) (Fig. 2*C*). By combining these observations with the fact that the low FRET state corresponds to the R-loop complex, we concluded that the observed transition from the low FRET state to the middle FRET state represents the unwinding of the target DNA in the PAM-distal region, which contains the putative site at which TS cleavage occurs, by the Cas12a RNP (the unwound conformation of which is termed the U-state hereafter).

On the other hand, for the detection of a considerable number of the TS cleavage events we employed a reaction buffer containing a high concentration of Mg^{2+} ions (10 mM). In the case of native DNA, we observed that the Cas12a ternary complex proceeded to the high FRET state (~0.59), in which the TS was cleaved and the cleaved DNA products were simultaneously released, as reported in our previous study (*SI Appendix*, Fig. S1*A*) (37). However, when we used a phosphorothiolate-modified TS to abolish the TS cleavage activity (termed TS noncleavable DNA) (33, 43), a clear two-state dynamics between middle FRET (~0.38, U-state) and high FRET (~0.59) states occurred but the release events did not (*SI Appendix*, Fig. S1*B*). This result indicates that the high FRET state represents a TS precleavage complex and that the TS cleavage event occurs in the high FRET state. In addition, when excess nonspecific single-stranded DNA substrates were added to prevent the exposed TS from binding to the RuvC catalytic site through competition, transition from the middle FRET state (U-state) to the high FRET state was impeded (Fig. 2 *D* and *E* and *SI Appendix*, Fig. S2). Based on these two observations, we concluded that the high FRET state represents the binding of the exposed TS to the catalytic site of the RuvC domain (termed B-state hereafter), which primes the TS for cleavage. Taken together, the results strongly suggest that the Cas12a–crRNA–DNA ternary complex undergoes two sequential conformational rearrangements, which illustrates the additional unwinding of the dsDNA region containing the putative site at which TS cleavage occurs and the subsequent binding of the exposed TS cleavage site to the catalytic site in the RuvC domain for complete dsDNA target cleavage.

PAM-Distal DNA Unwound Conformation Is Highly Stabilized by Mg^{2+}. Previous studies reported that Mg^{2+} ions coordinated in the RuvC catalytic pocket of Cas12 proteins are essential to create breaks in the dsDNA (10, 32, 44, 45). An in vitro DNA cleavage assay consistently showed that the TS cleavage efficiency of Cas12a RNPs was positively correlated with the Mg^{2+} concentration (Fig. 3*D* and *SI Appendix*, Fig. S3). In addition, similar results were obtained in single-molecule and bulk studies of the NTS cleavage reaction (*SI Appendix*, Figs. S4 and S5). Based on these findings, we asked whether Mg^{2+} ions are also involved in the two consecutive conformational rearrangements observed in the above experiments. To address this question, we performed Mg^{2+} titration experiments.

On the basis of our single-molecule observations, we derived a kinetic scheme for the TS cleavage reaction by Cas12a RNP, as shown in Fig. 3*A*. Using the unique capability of our single-molecule FRET assay to monitor these individual reaction steps in real time, we investigated the dependence of all transition rates in our kinetic scheme on the Mg^{2+} concentration. Representative time traces and the corresponding transition density plots (TDPs) obtained from the analysis of the time traces using hidden Markov modeling (HMM) are shown in Fig. 3*B* at varying Mg^{2+} concentration. As the Mg^{2+} concentration increased, the Cas12a ternary complex was biased toward transitioning to the forward states in our kinetic scheme (Fig. 3 *B* and *C*). Similar dynamic behavior was also observed in a wild-type DNA construct, not prenicked DNA constructs (*SI Appendix*, Fig. S6).

To determine which reaction step is the main determinant of Mg^{2+}-dependent TS cleavage, we obtained rate constants for all the transitions in our kinetic scheme at varying Mg^{2+} concentration (Fig. 3 *E* and *F*). Interestingly, in this observation the PAM-distal rewinding (k_{-1}) and TS cleavage (k_3) rates significantly correlated with the TS cleavage efficiencies at varying Mg^{2+} concentration, whereas the correlation of the remaining rate constants with the TS cleavage efficiencies was unappreciable. Notably, the strongest correlation of the PAM-distal rewinding rate (k_{-1}) with the Mg^{2+}-dependent TS cleavage efficiency revealed the unexpected structural role of Mg^{2+} ions in the TS cleavage reaction by Cas12a RNP, namely that Mg^{2+} ions contribute to stabilize the unwound conformation of the PAM-distal DNA (U-state). At the same time, the TS cleavage rate (k_3) was also correlated with the TS cleavage efficiency to an appreciable extent, which is reasonably predictable considering the traditional view that the Mg^{2+} ions coordinated to the RuvC domain play a catalytic role (44). Consequently, we strongly suggest that the unwinding of PAM-distal DNA acts as the main determinant of the Mg^{2+}-dependent TS cleavage via the allosteric mechanism that Mg^{2+} ions stabilize the unwound conformation and thereby promote binding and cleavage of the TS (Fig. 3 *C* and *D* and *SI Appendix*, Fig. S7).

Discussion

The transient and multistate nature of the TS cleavage reaction by Cas12a RNP occurring only after the NTS cleavage event has hindered a comprehensive understanding its underlying mechanisms due to population averaging that is inherent in ensemble measurements. Therefore, we used single-molecule FRET method that allows the direct visualization of the conformational rearrangements expected as essential prerequisites for the TS cleavage reaction. The single-molecule FRET assay described in this study allowed us to unravel the molecular mechanism underlying the regulation of the TS cleavage

Downloaded by guest on December 5, 2021

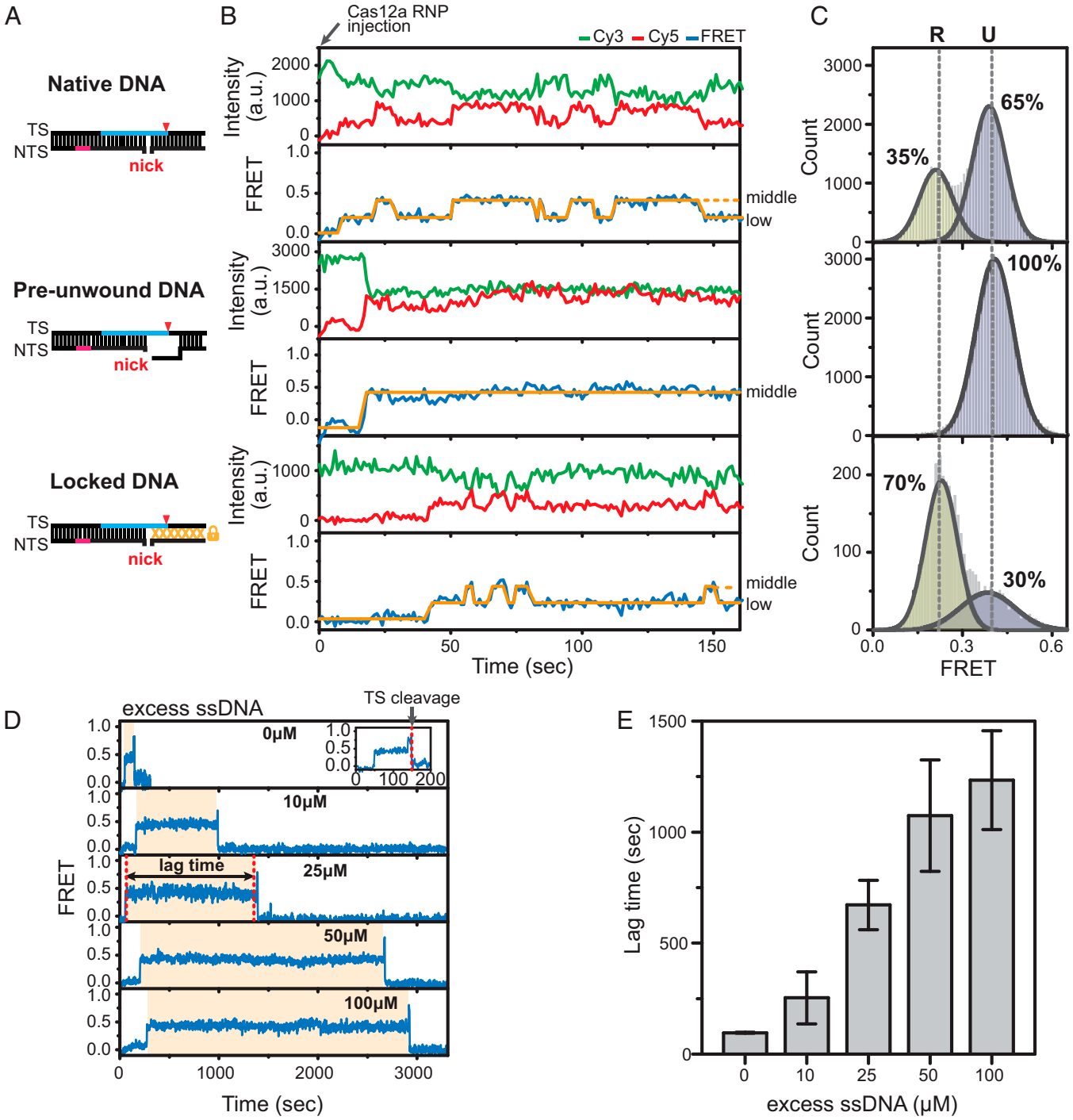


Fig. 2. Defining conformational intermediates in the TS cleavage reaction. (*A*) NTS prenicked DNA constructs (native DNA, *Top*; preunwound DNA, *Middle*; locked DNA, *Bottom*) used for the experiments to assign the FRET states to functional intermediates. (*B* and *C*) Representative intensity and FRET time traces showing conformational dynamics of the Cas12a–crRNA–DNA complex in the TS cleavage reaction (*B*) and corresponding FRET histograms of the Cas12a ternary complex (*C*) for three NTS prenicked DNA constructs (native DNA, *Top*; preunwound DNA, *Middle*; locked DNA, *Bottom*) in the presence of 20 nM Cas12a RNP and 0.5 mM Mg^{2+}. FRET histograms were obtained by collecting all data points for each DNA construct from at least more than 70 time traces. The relative population of each FRET intermediate was obtained by fitting the FRET histogram to the sum of two Gaussian functions. (*D*) Representative FRET time traces in the presence of 20 nM Cas12a RNP, 10 mM Mg^{2+}, and excess 13-nt single-stranded DNA (ssDNA) substrate with varying concentrations. (*E*) Lag times of transitions to the high FRET state in the absence and presence of excess 13-nt ssDNA substrate with varying concentrations (10, 25, 50, and 100 μM). The lag times were obtained by fitting the data to a single exponential decay function. The error bars in *E* were obtained from at least more than two independent experiments.

following the cleavage of NTS, which is summarized in Fig. 4 and below.

Initially, the Cas12a–crRNA–DNA complex maintains its R-loop conformation even after the NTS cleavage event. Next, owing to the strict single-stranded substrate specificity of the RuvC nuclease domain of Cas12a (7, 9, 13, 38), the PAM-distal region of target DNA is further unwound to expose the putative site at which TS cleavage occurs. Our rigorous kinetic

Downloaded by guest on December 5, 2021

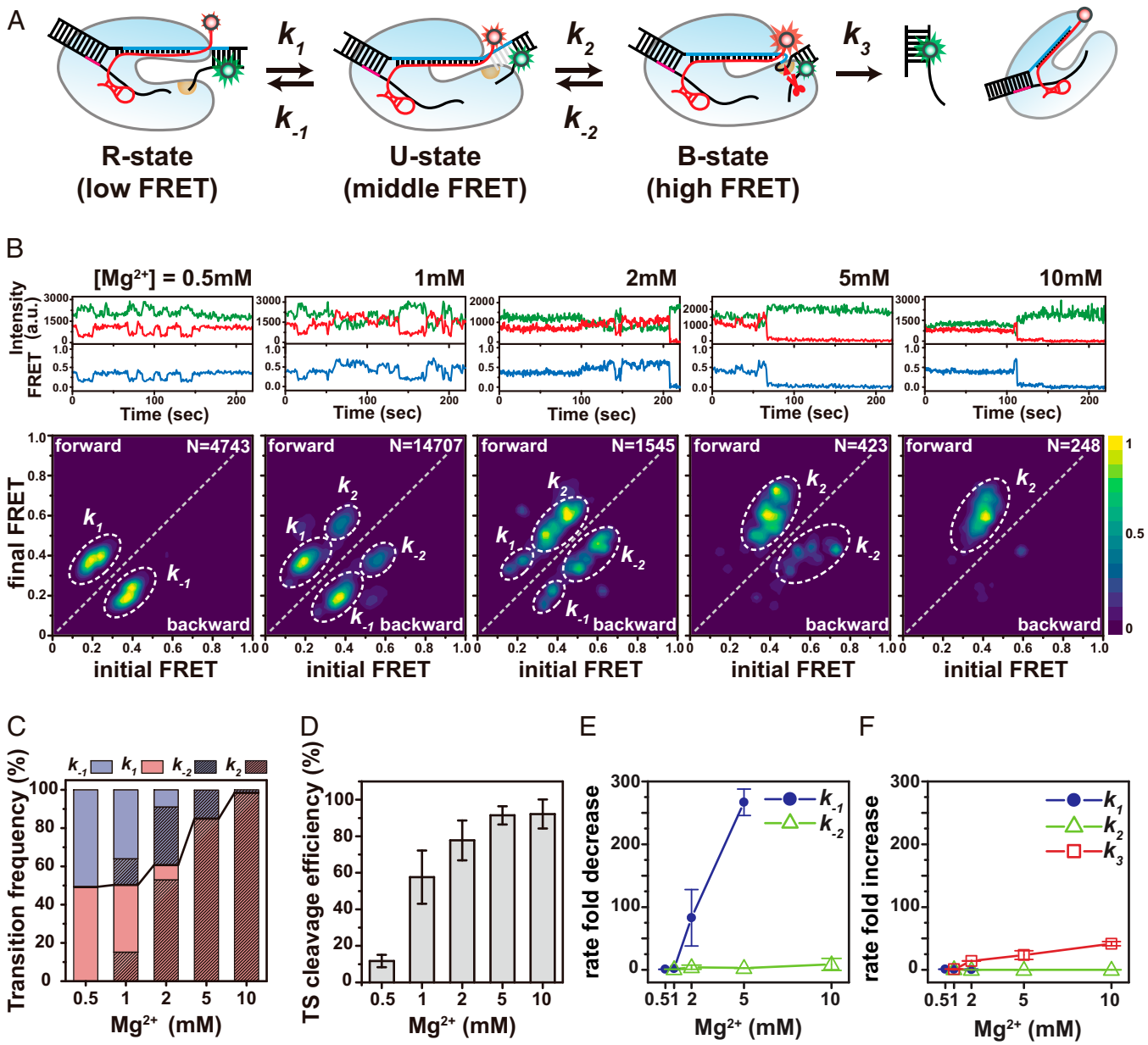


Fig. 3. Unwinding of PAM-distal DNA as the main determinant of the Mg^{2+}-dependent TS cleavage by Cas12a RNP. (*A*) Kinetic scheme for the cleavage reaction of the TS by Cas12a RNP. (*B*) Representative intensity and FRET time traces showing conformational dynamics of the Cas12a ternary complex (*Top*) and corresponding TDPs from HMM analysis of the time traces (*Bottom*) in the presence of 20 nM Cas12a RNP and Mg^{2+} ions with varying concentrations. In the TDPs, the FRET values before and after each transition were plotted as a normalized heat map. Dashed circles were added to clearly visualize the transitions between the three distinct FRET states. The total number of data points used in the analysis (N) is shown in each panel. The irreversible transition corresponding the TS cleavage and release (k_3) was not plotted in these plots. Instead, the relative population for the transition (k_3) compared to those of other transitions was shown in *SI Appendix*, Table S2. (*C*) Frequencies of each transition collected inside the circles drawn in the TDPs at varying Mg^{2+} concentration. (*D*) The TS cleavage efficiency obtained from the in vitro DNA cleavage assay at varying Mg^{2+} concentration. The error bars in *D* were obtained from three independent experiments. (*E*) Fold decrease in the PAM-distal rewinding (k_{-1}, blue circles) and TS unbinding (k_{-2}, green triangles) rates at varying Mg^{2+} concentration. (*F*) Fold increase in the PAM-distal unwinding (k_1, blue circles), TS binding (k_2, green triangles), and TS cleavage (k_3, red squares) rates at varying Mg^{2+} concentration. In *E* and *F*, some of rate constants (k_2, k_{-2}, and k_3 at 0.5 mM Mg^{2+} concentration; k_1 at Mg^{2+} concentration above 5 mM; k_{-1} at 10 mM Mg^{2+} concentration) were not obtained since the correponding transition events rarely occurred. Thus, k_1 and k_{-1} were normalized to the corresponding values at 0.5 mM Mg^{2+} concentration, and the remaining rates (k_2, k_{-2} and k_3) were normalized to the corresponding values at 1 mM Mg^{2+} concentration. All experimentally determined rate constants were plotted on the *y* axes in units of fold increase or decrease at each rate. For clarity, all datasets presented here are provided in *SI Appendix*, Table S3. Error bars in *E* and *F* were obtained from at least more than two independent experiments.

analysis of the conformational dynamics of this reaction step reveals that an increase in the Mg^{2+} concentration increases the energy barrier for rewinding the PAM-distal DNA and the free energy level of the unwound conformation of the PAM-distal DNA is deepened by increasing the Mg^{2+} concentration. This result unveiled the unexpected structural role of Mg^{2+} ions in stabilizing the unwound conformation of the PAM-distal DNA. Once the unwound conformation of the PAM-distal DNA stabilizes, the exposed putative cleavage site in the TS binds to the catalytic center of the RuvC nuclease domain of

Downloaded by guest on December 5, 2021

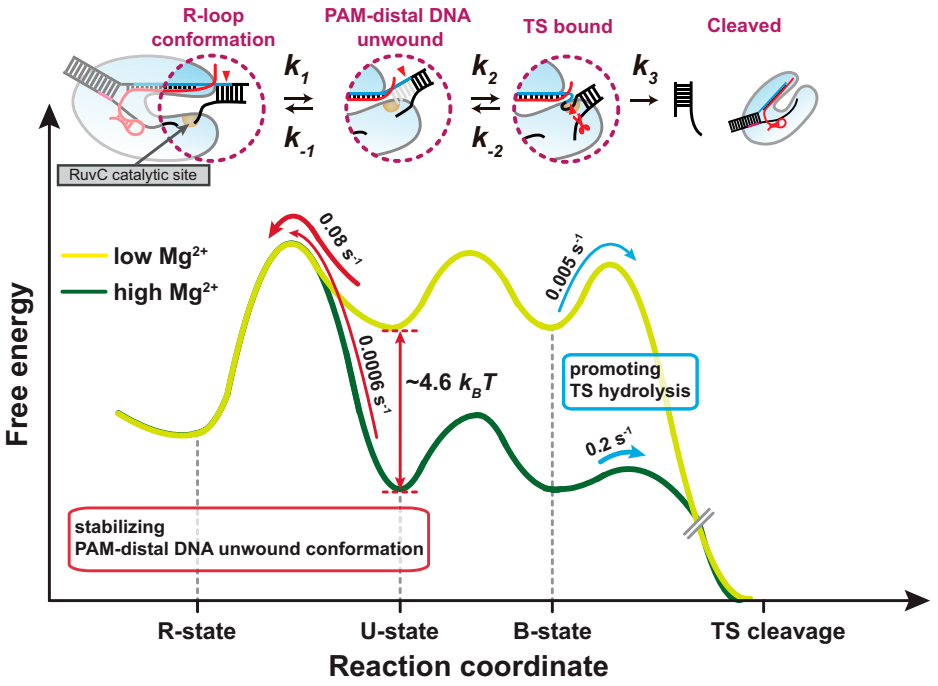


Fig. 4. Proposed model for Mg^{2+}-dependent conformational rearrangements in the TS cleavage reaction by Cas12a RNP. Cartoon free energy landscapes for the Cas12a–crRNA–DNA complex during the TS cleavage reaction at high (dark green line, 5 mM) and low (light green line, 1 mM) Mg^{2+} ion concentrations were estimated based on the experimentally determined rate constants for all possible transitions in the TS cleavage reaction. A detailed description of the estimation method is provided in *Materials and Methods*. The energy barrier for the PAM-distal DNA rewinding is raised by an increase in Mg^{2+} concentration, and that for the TS cleavage step is lowered by an increase in Mg^{2+} concentration.

Cas12a, whereby the TS is finally cleaved by the RuvC domain. Our kinetic data suggest that the energy barrier for the TS cleavage in this step is also significantly lowered by an increase in the Mg^{2+} concentration.

In conclusion, we found that the TS cleavage reaction of Cas12a RNP proceeds via two consecutive conformational rearrangements that were identified as the local unwinding of the PAM-distal region and the subsequent binding of the exposed TS to the catalytic site. In particular, we strongly suggest that the additional unwinding of the target DNA in the PAM-distal region is a crucial reaction step en route to the TS cleavage, which is allosterically stabilized by Mg^{2+} ions. This mechanistic insight afforded by our study enables a rational strategy for Cas12a engineering to abolish the TS cleavage activity including alterations of the guide RNA in the PAM-distal region or mutations of residues relevant to the PAM-distal DNA unwinding or the TS binding, except for the metal-coordinating residues. This would enable the development of engineered Cas12a RNPs having a complete nickase activity to extend the range of genome editing applications.

Materials and Methods

Expression and Purification of AsCas12a. The recombinant protein plasmid was transformed into BL21-Pro cells (CP111; Enzynomics) and single colonies were isolated on an agar plate containing kanamycin. A single colony was inoculated in lysogeny broth medium containing kanamycin and grown at 37 °C with shaking at 200 rpm to optical density at 600 nm ~0.4 to 0.5. The cells were then induced with 0.8 mM isopropyl β-D-1-thiogalactopyranoside and incubated at 18 °C overnight with shaking at 200 rpm. Cells were harvested by centrifugation at 6,000 × *g* for 10 min at 4 °C and resuspended in cell lysis buffer containing 50 mM NaH_2PO_4, 300 mM NaCl, and 10 mM imidazole. A lysozyme and 1 mM phenylmethanesulfonyl fluoride were added and the solution was incubated on ice for 1 h. Cells were repeatedly sonicated (five times) and the lysate was centrifuged at 18,000 × *g* for 30 min at 4 °C. The supernatant was filtered through a 0.45-μm filter and incubated with Ni-NTA agarose with rotation for 1 h at 4 °C. The resin was washed twice with wash buffer containing 50 mM NaH_2PO_4, 300 mM NaCl, and 20 mM imidazole and the protein was eluted with elution buffer (50 mM NaH_2PO_4, 300 mM NaCl, and 250 mM imidazole). The eluted protein was further purified using protein concentrator (100,000 molecular weight cutoff) and diluted with storage buffer containing 20 mM Hepes, 150 mM NaCl, 0.1 mM ethylenediaminetetraacetic acid (EDTA), 1 mM dithiothreitol (DTT), 2% sucrose, and 20% glycerol.

DNA and RNA Preparation. The DNA and RNA oligonucleotides used in this study (as shown in *SI Appendix*, Table S1) were purchased from Integrated DNA technology with high-performance liquid chromatography (HPLC) purification. Nontarget DNA strands for single-molecule FRET experiments were labeled with Cy3 NHS-ester dye (GE Healthcare) at the amine group of an internal amino modifier (dTC6). To construct the target DNA duplexes for single-molecule FRET experiments, complementary DNA strands were annealed by incubation at 95 °C for 5 min, followed by slow cooling of the mixture of the biotinylated TS and the Cy3-labeled NTS (1:2 molar ratio) in a buffer containing 10 mM Tris·HCl (pH 8.0) and 50 mM NaCl. Some of the HPLC-purified crRNA strands were labeled with Cy5 at the 3′ end of the strand for single-molecule FRET experiments. To construct target DNA duplexes for in vitro DNA cleavage assay, complementary DNA strands were annealed by incubation at 95 °C for 5 min, followed by slow cooling of the mixture of the Cy3-labeled TS and the nonlabeled NTS (1:1 molar ratio) in a buffer containing 10 mM Tris·HCl (pH 8.0) and 50 mM NaCl.

In Vitro DNA Cleavage Assay by Cas12a. The purified Cas12a and crRNA were mixed in a 1:1 molar ratio to prepare a final Cas12a RNP concentration of 1 μM and incubated at 37 °C for 5 min in a reaction buffer to form a Cas12a RNP complex, and then the NTS prenicked DNA target was added to the reaction buffer. The final 15-μL reaction buffer contained 1 μM Cas12a, 1 μM crRNA, 100 nM Cy3-labeled NTS prenicked DNA, 10 mM Tris·HCl, pH 8.0, 100 mM NaCl, 1 mM DTT, and varying concentrations of $MgCl_2$ and was incubated at 37 °C for 10 min. The cleavage reactions were stopped by adding 2 μg of Proteinase K (Thermo Fisher Scientific) followed by incubation at 37 °C for 5 min. The samples were loaded in 15% TBE-Urea gel with TBE-UREA sample buffer (45 mM Tris·HCl, pH 8.0, 45 mM boric acid, 10 mM EDTA, 6% Ficoll type 400, 3.5 M urea, and 0.25% xylene cyane). The fluorescent signal from the Cy3-labeled TS was detected using the ChemiDoc MP system (Bio-Rad). Experiments were independently performed in triplicate. The TS cleavage efficiencies shown in Fig. 3*D* were quantified using Image Lab (Bio-Rad). On the other

Downloaded by guest on December 5, 2021

hand, 0.2 μM Cas12a, 0.2 μM crRNA, and 20 nM Cy5-labeled TS prenicked DNA were used in the DNA cleavage assay to obtain the NTS cleavage efficiencies as shown in *SI Appendix*, Fig. S5.

Single-Molecule FRET Experiments. Single-molecule FRET experiments were performed using a sample chamber constructed with a quartz slide and coverslip (46). To prevent undesirable adsorption of proteins to the surface, the quartz slide and coverslip were thoroughly cleaned and coated with polyethylene glycol (PEG) and biotinylated PEG (Laysan Bio) in a 40:1 ratio. The biotinylated target DNA duplexes were immobilized on the PEG-coated surface of the chamber via a streptavidin–biotin interaction. Single-molecule fluorescence images were obtained using a home-built prism-type total internal reflection fluorescence microscope with 1-s time resolution unless mentioned otherwise. To reduce photobleaching and blinking of the fluorophores, a glucose-coupled glucose oxidase/catalase (GODCAT) oxygen-scavenging system and a blinking suppressant (Trolox) were used (47). All single-molecule FRET measurements were performed at 37 °C under the following buffer conditions unless mentioned otherwise: 10 mM Tris·HCl (pH 8.0), 100 mM NaCl, 0.9 mM EDTA, 1 mM DTT, varying concentrations of $MgCl_2$, and an oxygen scavenging system (0.4% [wt/vol] glucose [Sigma], 1% [vol/vol] Trolox [Sigma], 1 mg/mL glucose oxidase [Sigma], and 0.04 mg/mL catalase [Roche]). To monitor the conformational dynamics throughout the TS cleavage reaction by Cas12a RNP, a new reaction buffer containing 20 nM of Cas12a RNPs (unless mentioned otherwise) was introduced into the detection chamber in real time by using a syringe pump (Fusion 200; Chemyx) while single-molecule images were being taken under excitation of Cy3 by a green laser (532-nm, sapphire; Coherent). Fluorescence signals from Cy3 and Cy5 were collected by a water immersion objective lens (UPlanSApo ×60; Olympus), filtered through a 532-nm notch filter (NF03-532E-25; Semrock) to reject scattered excitation laser lines, separated with a dichroic mirror (635dcxr; Chroma), and imaged onto an electron-multiplying charged-coupled device camera (Ixon Ultra DU897U; Andor).

Analysis of Single-Molecule FRET Data. Time courses of Cy3 and Cy5 signals from a single Cas12a–crRNA–DNA complex were extracted from a recorded movie using scripts written in IDL software (ITT Visual Information Solutions) and analyzed using custom software written in MATLAB (MathWorks) (48). FRET efficiency, defined as the ratio of acceptor (Cy5) intensity to the sum of donor (Cy3) and acceptor intensities, was calculated in consideration of background noise and bleed-through of the donor signal to the acceptor channel. After data correction, we selected real molecule traces showing anticorrelations between the donor and acceptor or single-step photobleaching.

Determination of Kinetic Rate Constants. To obtain the kinetic times from the time traces, FRET states for individual reaction steps were determined using HMM (49). Dwell-time histograms of each state were fitted by an exponential decay function to obtain the corresponding kinetic times (*SI Appendix*, Fig. S8). Due to reversibility of the transitions between multiple intermediates of the TS cleavage reaction as depicted in Fig. 3*A*, two conformational intermediates, the PAM-distal DNA unwound state (U-state) and the TS bound state (B-state), have two competing reaction pathways, respectively, as follows: TS binding (k_2) and PAM-distal rewinding (k_{-1}) for U-state and TS cleavage (k_3) and TS unbinding (k_{-2}) for B-state. Hence, the inverse of dwell time for U-state provides the sum of TS binding (k_2) and PAM-distal rewinding (k_{-1}) rates, which is multiplied by the relative frequency of each transition event to obtain individual TS binding (k_2) and PAM-distal rewinding (k_{-1}) rates (*SI Appendix*, Table S2) (50, 51). In the same way, the inverse of dwell time for the B-state also provides the sum of TS cleavage (k_3) and TS unbinding (k_{-2}) rates, which is multiplied by the relative frequency of each transition event to obtain the two reaction rate constants. In addition, the remaining PAM-distal unwinding rate (k_1) is determined by merely inverting the corresponding dwell time.

Estimation for Free Energy Landscapes. To draw free energy landscapes, first the free energy of the initial R-state was set to 0 k_BT. Then, free energy difference ΔG^0_{ij} between the states (i, j = R, U, and B-state) was determined via following equation:

$$\Delta G^0_{ij} = -k_B T \cdot \ln K_{eq,ij},$$

where k_B is the Boltzman constant, T is the temperature, and $K_{eq,ij}$ is the equilibrium constant between i and j states.

Next, the relative free energy barrier (or activation energy, $E_{a,ij}$) for the transition between i and j states was estimated using Arrhenius equation, $k_{ij} = A \cdot e^{-E_{a,ij}/k_BT}$, even though it was not feasible to directly calculate the energy barrier because the pre-exponential constant A could not be determined.

Data Availability. Custom-written programs for small-molecule FRET data acquisition have been deposited in GitHub (https://github.com/pjb7687/single). All other study data are included in the article and/or *SI Appendix*.

ACKNOWLEDGMENTS. This work was supported by National Research Foundation of Korea Grants 2019R1C1C1008438, 2020M3A9I4038197, and 2021R1A2C1007593 funded by the Ministry of Science and ICT of the Korean Government and by a Gwangju Institute of Science and Technology (GIST) Research Institute grant funded by GIST.

1. M. Jinek *et al.*, A programmable dual-RNA-guided DNA endonuclease in adaptive bacterial immunity. *Science* **337**, 816–821 (2012).
2. G. Gasiunas, R. Barrangou, P. Horvath, V. Siksnys, Cas9-crRNA ribonucleoprotein complex mediates specific DNA cleavage for adaptive immunity in bacteria. *Proc. Natl. Acad. Sci. U.S.A.* **109**, E2579–E2586 (2012).
3. L. Cong *et al.*, Multiplex genome engineering using CRISPR/Cas systems. *Science* **339**, 819–823 (2013).
4. P. D. Hsu, E. S. Lander, F. Zhang, Development and applications of CRISPR-Cas9 for genome engineering. *Cell* **157**, 1262–1278 (2014).
5. J. A. Doudna, E. Charpentier, Genome editing. The new frontier of genome engineering with CRISPR-Cas9. *Science* **346**, 1258096 (2014).
6. G. J. Knott, J. A. Doudna, CRISPR-Cas guides the future of genetic engineering. *Science* **361**, 866–869 (2018).
7. B. Paul, G. Montoya, CRISPR-Cas12a: Functional overview and applications. *Biomed. J.* **43**, 8–17 (2020).
8. T. Swartjes, R. H. J. Staals, J. van der Oost, Editor's cut: DNA cleavage by CRISPR RNA-guided nucleases Cas9 and Cas12a. *Biochem. Soc. Trans.* **48**, 207–219 (2020).
9. D. C. Swarts, M. Jinek, Cas9 versus Cas12a/Cpf1: Structure-function comparisons and implications for genome editing. *Wiley Interdiscip. Rev. RNA*, **2018**, e1481 (2018).
10. B. Zetsche *et al.*, Cpf1 is a single RNA-guided endonuclease of a class 2 CRISPR-Cas system. *Cell* **163**, 759–771 (2015).
11. S. Stella, P. Alcón, G. Montoya, Structure of the Cpf1 endonuclease R-loop complex after target DNA cleavage. *Nature* **546**, 559–563 (2017).
12. I. Fonfara, H. Richter, M. Bratovič, A. Le Rhun, E. Charpentier, The CRISPR-associated DNA-cleaving enzyme Cpf1 also processes precursor CRISPR RNA. *Nature* **532**, 517–521 (2016).
13. J. S. Chen *et al.*, CRISPR-Cas12a target binding unleashes indiscriminate single-stranded DNase activity. *Science* **360**, 436–439 (2018).
14. B. Zetsche *et al.*, Multiplex gene editing by CRISPR-Cpf1 using a single crRNA array. *Nat. Biotechnol.* **35**, 31–34 (2017).
15. D. Kim *et al.*, Genome-wide analysis reveals specificities of Cpf1 endonucleases in human cells. *Nat. Biotechnol.* **34**, 863–868 (2016).
16. X. Tang *et al.*, A CRISPR-Cpf1 system for efficient genome editing and transcriptional repression in plants. *Nat. Plants* **3**, 17103 (2017).
17. B. P. Kleinstiver *et al.*, Genome-wide specificities of CRISPR-Cas Cpf1 nucleases in human cells. *Nat. Biotechnol.* **34**, 869–874 (2016).
18. J. S. Gootenberg *et al.*, Multiplexed and portable nucleic acid detection platform with Cas13, Cas12a, and Csm6. *Science* **360**, 439–444 (2018).
19. S. Y. Li *et al.*, CRISPR-Cas12a-assisted nucleic acid detection. *Cell Discov.* **4**, 20 (2018).
20. J. P. Broughton *et al.*, CRISPR-Cas12-based detection of SARS-CoV-2. *Nat. Biotechnol.* **38**, 870–874 (2020).
21. Y. Li, S. Li, J. Wang, G. Liu, CRISPR/Cas systems towards next-generation biosensing. *Trends Biotechnol.* **37**, 730–743 (2019).
22. A. V. Anzalone, L. W. Koblan, D. R. Liu, Genome editing with CRISPR-Cas nucleases, base editors, transposases and prime editors. *Nat. Biotechnol.* **38**, 824–844 (2020).
23. A. V. Anzalone *et al.*, Search-and-replace genome editing without double-strand breaks or donor DNA. *Nature* **576**, 149–157 (2019).
24. H. A. Rees, D. R. Liu, Base editing: Precision chemistry on the genome and transcriptome of living cells. *Nat. Rev. Genet.* **19**, 770–788 (2018).
25. B. P. Kleinstiver *et al.*, Engineered CRISPR-Cas12a variants with increased activities and improved targeting ranges for gene, epigenetic and base editing. *Nat. Biotechnol.* **37**, 276–282 (2019).
26. D. Kim, K. Lim, D. E. Kim, J. S. Kim, Genome-wide specificity of dCpf1 cytidine base editors. *Nat. Commun.* **11**, 4072 (2020).
27. X. Li *et al.*, Base editing with a Cpf1-cytidine deaminase fusion. *Nat. Biotechnol.* **36**, 324–327 (2018).
28. C. C. Campa, N. R. Weisbach, A. J. Santinha, D. Incarnato, R. J. Platt, Multiplexed genome engineering by Cas12a and CRISPR arrays encoded on single transcripts. *Nat. Methods* **16**, 887–893 (2019).
29. K. Murugan, A. S. Seetharam, A. J. Severin, D. G. Sashital, CRISPR-Cas12a has widespread off-target and dsDNA-nicking effects. *J. Biol. Chem.* **295**, 5538–5553 (2020).
30. T. Yamano *et al.*, Crystal structure of Cpf1 in complex with guide RNA and target DNA. *Cell* **165**, 949–962 (2016).

Downloaded by guest on December 5, 2021

31. S. Stella *et al.*, Conformational activation promotes CRISPR-Cas12a catalysis and resetting of the endonuclease activity. *Cell* **175**, 1856–1871.e21 (2018).
32. D. C. Swarts, J. van der Oost, M. Jinek, Structural basis for guide RNA processing and seed-dependent DNA targeting by CRISPR-Cas12a. *Mol. Cell* **66**, 221–233.e4 (2017).
33. D. C. Swarts, M. Jinek, Mechanistic insights into the cis- and trans-acting DNase activities of Cas12a. *Mol. Cell* **73**, 589–600.e4 (2019).
34. I. Strohkendl, F. A. Saifuddin, J. R. Rybarski, I. J. Finkelstein, R. Russell, Kinetic basis for DNA target specificity of CRISPR-Cas12a. *Mol. Cell* **71**, 816–824.e3 (2018).
35. D. Singh *et al.*, Real-time observation of DNA target interrogation and product release by the RNA-guided endonuclease CRISPR Cpf1 (Cas12a). *Proc. Natl. Acad. Sci. U.S.A.* **115**, 5444–5449 (2018).
36. L. Zhang *et al.*, Conformational dynamics and cleavage sites of Cas12a are modulated by complementarity between crRNA and DNA. *iScience* **19**, 492–503 (2019).
37. Y. Jeon *et al.*, Direct observation of DNA target searching and cleavage by CRISPR-Cas12a. *Nat. Commun.* **9**, 2777 (2018).
38. J. C. Cofsky *et al.*, CRISPR-Cas12a exploits R-loop asymmetry to form double-strand breaks. *eLife* **9**, e55143 (2020).
39. D. Dong *et al.*, The crystal structure of Cpf1 in complex with CRISPR RNA. *Nature* **532**, 522–526 (2016).
40. P. Gao, H. Yang, K. R. Rajashankar, Z. Huang, D. J. Patel, Type V CRISPR-Cas Cpf1 endonuclease employs a unique mechanism for crRNA-mediated target DNA recognition. *Cell Res.* **26**, 901–913 (2016).
41. E. Wörle, L. Jakob, A. Schmidbauer, G. Zinner, D. Grohmann, Decoupling the bridge helix of Cas12a results in a reduced trimming activity, increased mismatch sensitivity and impaired conformational transitions. *Nucleic Acids Res.* **49**, 5278–5293 (2021).
42. H. Yang, P. Gao, K. R. Rajashankar, D. J. Patel, PAM-dependent target DNA recognition and cleavage by C2c1 CRISPR-Cas endonuclease. *Cell* **167**, 1814–1828.e12 (2016).
43. F. Eckstein, G. Gish, Phosphorothioates in molecular biology. *Trends Biochem. Sci.* **14**, 97–100 (1989).
44. J. S. Chen, J. A. Doudna, The chemistry of Cas9 and its CRISPR colleagues. *Nat. Rev. Chem.* **1**, 0078 (2017).
45. X. Huang *et al.*, Structural basis for two metal-ion catalysis of DNA cleavage by Cas12i2. *Nat. Commun.* **11**, 5241 (2020).
46. R. Roy, S. Hohng, T. Ha, A practical guide to single-molecule FRET. *Nat. Methods* **5**, 507–516 (2008).
47. I. Rasnik, S. A. McKinney, T. Ha, Nonblinking and long-lasting single-molecule fluorescence imaging. *Nat. Methods* **3**, 891–893 (2006).
48. S. Lee, Y. Jang, S. J. Lee, S. Hohng, Single-molecule multicolor FRET assay for studying structural dynamics of biomolecules. *Methods Enzymol.* **581**, 461–486 (2016).
49. S. A. McKinney, C. Joo, T. Ha, Analysis of single-molecule FRET trajectories using hidden Markov modeling. *Biophys. J.* **91**, 1941–1951 (2006).
50. M. K. Nahas *et al.*, Observation of internal cleavage and ligation reactions of a ribozyme. *Nat. Struct. Mol. Biol.* **11**, 1107–1113 (2004).
51. Y. Jang *et al.*, Selection of DNA cleavage sites by topoisomerase II results from enzyme-induced flexibility of DNA. *Cell Chem. Biol.* **26**, 502–511.e3 (2019).

Downloaded by guest on December 5, 2021